

# Electronic structure of the $MO$ oxides ( $M=\text{Mg, Ca, Ti, V}$ ) in the GW approximation

Atsushi Yamasaki\* and Takeo Fujiwara†

*Department of Applied Physics, University of Tokyo, Bunkyo-ku, Tokyo 113-8656, Japan*

(Dated: published 13 December 2002)

The quasiparticle band structures of nonmagnetic monoxides,  $MO$  ( $M=\text{Mg, Ca, Ti, and V}$ ), are calculated by the GW approximation. The band gap and the width of occupied oxygen  $2p$  states in insulating MgO and CaO agree with experimental observation. In metallic TiO and VO, conduction bands originated from metal  $3d$  states become narrower. Then the partial densities of transition metal  $e_g$  and  $t_{2g}$  states show an enhanced dip between the two. The effects of static screening and dynamical correlation are discussed in detail in comparison with the results of the Hartree-Fock approximation and the static Coulomb hole plus screened exchange approximation. The  $d$ - $d$  Coulomb interaction is shown to be very much reduced by on-site and off-site  $d$ -electron screening in TiO and VO. The dielectric function and the energy loss spectrum are also presented and discussed in detail.

PACS numbers: 71.10.-w, 71.15.-m, 71.20.Be

## I. INTRODUCTION

The first-principle electronic structure calculation, based on the local-density approximation (LDA) within the density-functional theory (DFT),<sup>1</sup> has had great success in theoretical investigations of the ground state property of condensed matters. However, in many LDA calculations, the band gap is unsatisfactory underestimated in insulators and semiconductors. In the electronic structure of  $3d$  transition metals calculated by the LDA, the occupied  $3d$  band width is too broad, the exchange splitting is overestimated and the satellite structure in the x-ray photoemission spectroscopy (XPS) does not appear. These quantities are associated with quasiparticle properties. The transition metal monoxides  $TO$  ( $T=\text{Mn, Fe, Co, and Ni}$ ) are wide-gap antiferromagnetic insulators in experiments, but FeO and CoO appear as metals, and MnO and NiO as small-gap semiconductors in the LDA.<sup>2</sup> The magnetic moments of  $TO$  are underestimated by the LDA.

The electronic structure in strongly correlated electron systems has been highly challenging field. The self-Coulomb and self-exchange interactions almost cancel with each other in many cases of the LDA but still not completely in  $TO$ .<sup>3</sup> The self-interaction corrected LDA (SIC-LDA) has been applied to transition metal monoxides.<sup>4,5</sup> It gives satisfactory results for the band gap and magnetic moments in the transition metal monoxides  $TO$  ( $\text{Tr}=\text{Mn, Fe, Co, and Ni}$ ) except VO. The LDA+U method<sup>6,7,8</sup> works reasonably well for the Mott-Hubbard insulators or rare earth metal compounds where the  $3d$  or  $4f$  bands are partially filled. The LDA+U method is a static limit of the GW approximation (GWA).<sup>8</sup> However, application of the LDA+U method to early transition metal monoxides TiO and VO would lead to antiferromagnetic insulators rather than paramagnetic metals.<sup>6</sup>

The GWA is the first term approximation of the many-body perturbation series for the Green function, and is a simple but excellent method to calculate the self-energy with the dynamical correlation.<sup>9,10</sup> On the other hand,

the HF approximation overestimates the band gap in insulators and semiconductors because of the lack of the screening terms and gives zero density of states at the Fermi level in the electron gas. In the GWA, there is no self-interaction because the exchange term of the GWA is of the Hartree-Fock type. The dynamical correlation effect in the GWA is treated by the random-phase approximation (RPA). In the GWA, the dynamical effects give rise to important features that are not accounted for by the HF approximation, for example, damping of quasiparticles and characteristic structure in the spectral function. The screening effects recover the finite density of states at the Fermi level. The band gap is corrected and reduced in the GWA by the dynamical screening effects in comparison with the one of the HF approximation. The dynamical correlation effect is important for the band width in the transition metals.<sup>11</sup> We could not expect improvement in the GWA for the exchange splitting and satellite structure because it needs higher order diagrams (e.g., vertex corrections) for electron-electron and hole-hole scattering processes.<sup>12</sup>

The GWA has been applied to several real systems, for example, simple metals,<sup>13</sup> semiconductors and insulators,<sup>14,15,16</sup> transition metals,<sup>17</sup> and transition metal monoxides.<sup>18</sup> In simple metals and semiconductors, the GWA can be formulated with plane wave basis set based on the pseudopotential method and the plasmon pole approximation has been often used for calculating dielectric function.<sup>14</sup> In contrast, transition metals and their compounds have strong atomic potentials and the GWA based on the pseudopotential method cannot be applied because of restriction of the number of plane waves. It is essentially important to include core electrons in many cases and, moreover, the plasmon pole approximation is not applicable to the dielectric function for transition metals and their compounds because there is no isolated plasmon pole. Therefore, all-electron calculation and no plasmon-pole approximation in the dielectric function are required for transition metals and their compounds.

The GW calculation of Ni, based on the linearized

augmented-plane-wave (LAPW) basis and no approximation in the dielectric function, gives results in good agreement with experiments.<sup>17</sup> The modeling of the screened interaction in the GWA is able to explain satisfactorily photoemission spectra in MnO,<sup>19</sup> NiO,<sup>20</sup> and VO<sub>2</sub>.<sup>21</sup> In the pioneering work of the GW calculation of NiO by Aryasetiawan, the band gap and magnetic moment agree quite well with experimental values.<sup>18</sup> In the analysis of photoemission spectroscopy by the cluster configuration-interaction theory, NiO is assigned as a charge-transfer type insulator,<sup>22</sup> but in the LDA it is classified as a Mott-Hubbard type insulator because the transition metal  $3d$  bands appear at higher energy than oxygen  $2p$  bands.<sup>2</sup> The relative position of the oxygen  $2p$  states of the GWA is also improved in comparison with that of the LDA. However, the top of the valence bands in the GWA is mainly Ni  $3d$  states and NiO could not be a charge-transfer type insulator.

In most GW calculations, full self-consistency is not carried out. The self-consistency in the GW calculations can maintain the conservation laws of particle number, energy, and momentum.<sup>23</sup> However such treatment cannot guarantee better agreement with experimental results.<sup>24</sup>

Because it is derived from many-body perturbation theory, the GWA is applicable to wide variety of classes of systems, and should be tested in various systems. In this paper, the GW method based on the linear muffin-tin orbital (LMTO) method<sup>25</sup> is applied to several nonmagnetic oxides, insulating MgO, CaO and metallic TiO, VO. Only the electronic structure in MgO was calculated by the GWA before.<sup>16</sup> The insulators MgO and CaO are typical simple oxides, whose insulating band gap is underestimated by the LDA. TiO and VO are nonmagnetic metallic oxides. In the LDA their characteristics are very similar. We will discuss the electronic band structure and its systematic variation for MgO, CaO, TiO, and VO, concerning with the  $E$ - $\mathbf{k}$  relation, band gap, band width, the density of states, plasmon frequencies, structures in the energy loss spectrum, and other properties. We will also discuss the correlation effects, including the strength of the Coulomb interaction with  $d$ - $d$  screening effects.

The paper is organized as follows. A simple review on the theoretical framework will be given in Sec. II. The results for these systems are presented and discussed in Sec. III. The dielectric function and the energy loss spectrum are also discussed. Finally, in Sec. IV we present our summary.

## II. THEORY

### A. GW approximation

When effects of dynamical correlation are included, the self-energy is expressed formally as a series expansion of dynamically screened interaction. The GWA replaces the self-energy by the lowest order term of the expansion as

$\Sigma(1, 2) = iG(1, 2)W(1, 2)$ .  $G$  is the one particle Green function and the dynamically screened interaction  $W$  is defined by

$$W(1, 2) = \int d(3)\varepsilon^{-1}(1, 3)v(3, 2), \quad (1)$$

$$= v(1, 2) + \int d(34)v(1, 3)\chi^0(3, 4)W(4, 2), \quad (2)$$

$$= v(1, 2) + W^c(1, 2), \quad (3)$$

where  $\varepsilon$  is the dynamical dielectric function,  $v$  is the bare Coulomb potential and  $\chi^0$  is the irreducible polarization function  $\chi^0(1, 2) = -iG(1, 2)G(2, 1)$ . Here we use an abbreviated notation  $(1) = (\mathbf{r}_1, \sigma_1, t_1)$  and  $v(1, 2) = v(\mathbf{r}_1, \mathbf{r}_2)\delta(t_1 - t_2)$ . Equation (2) can be treated by the RPA.

We adopt the LDA Hamiltonian to be the unperturbed one  $H^0$ ,

$$H^0 = T + V^H + V_{\text{LDA}}^{\text{xc}}. \quad (4)$$

Here  $T$  is the kinetic energy,  $V^H$  is the Hartree potential, and  $V_{\text{LDA}}^{\text{xc}}$  is the exchange-correlation potential in the LDA. We presume the wave functions  $\{\psi_{\mathbf{k}n}(\mathbf{r})\}$  of the LDA to be a reasonably good starting wave functions, though this assumption should be carefully investigated in detail. Then the self-energy can be written by three terms as

$$\Delta\Sigma = \Sigma^x + \Sigma^c - V_{\text{LDA}}^{\text{xc}}, \quad (5)$$

where  $\Sigma^x (= iGv)$  is the exchange part (the Fock term) and  $\Sigma^c (= iGW^c)$  is the dynamical correlation part. The quasiparticle energy is given as

$$E_{\mathbf{k}n} = \epsilon_{\mathbf{k}n} + Z_{\mathbf{k}n}\Delta\Sigma_{\mathbf{k}n}(\epsilon_{\mathbf{k}n}), \quad (6)$$

where  $\epsilon_{\mathbf{k}n}$  is the LDA eigenvalue. The self-energy  $\Delta\Sigma_{\mathbf{k}n}$  and the renormalization factor  $Z_{\mathbf{k}n}$ , the weight of the spectral function, are given by

$$\Delta\Sigma_{\mathbf{k}n}(\epsilon_{\mathbf{k}n}) = \langle \psi_{\mathbf{k}n} | \Sigma^x + \Sigma^c(\epsilon_{\mathbf{k}n}) - V_{\text{LDA}}^{\text{xc}} | \psi_{\mathbf{k}n} \rangle, \quad (7)$$

$$Z_{\mathbf{k}n} = \left[ 1 - \left. \frac{\partial \Delta\Sigma_{\mathbf{k}n}(\omega)}{\partial \omega} \right|_{\omega=\epsilon_{\mathbf{k}n}} \right]^{-1}. \quad (8)$$

The renormalization factor  $Z_{\mathbf{k}n}$  is a measure of the occupation number and should equal to the discontinuity of occupation number at the Fermi energy. Therefore it should satisfy the condition  $Z_{\mathbf{k}n} \leq 1$ . In the present work we perform one iteration calculation without self-consistency.

In order to know the difference of the dynamical and static screening effects, we also apply the static Coulomb hole plus screened exchange (COHSEX) approximation for the self-energy by Hedin.<sup>9</sup> The static COHSEX approximation can be obtained by neglecting energy dependence of the self-energy. Then the self-energy is expressed

TABLE I: The band gap  $E_G$ , the width of valence band  $W_v$ , and the position of the O  $s$  band  $E_{O_s}$  in insulating MgO and CaO. The unit is (eV).

	MgO					CaO						
	LDA	HF			COHSEX	GWA	expt.	LDA	HF	COHSEX	GWA	expt.
$E_G$	5.2	18.4, <sup>a</sup>	16.5, <sup>b</sup>	17.6 <sup>c</sup>	9.6	8.2	7.8 <sup>d</sup>	3.65	15.9 <sup>c</sup>	7.7	6.64	7.1 <sup>d</sup>
$W_v$	5.0	10.4, <sup>a</sup>	5.8, <sup>b</sup>	7.64 <sup>c</sup>	5.6	5.0	5.0–6.0 <sup>d</sup>	2.8	3.43 <sup>c</sup>	3.4	2.9	
$E_{O_s}$	$\sim 16$	$\sim 40,a \sim 24c$			$\sim 19$	$\sim 17$	18–21 <sup>e</sup>	$\sim 15$		$\sim 17$	$\sim 16$	

<sup>a</sup>Reference 26.

<sup>b</sup>Reference 27.

<sup>c</sup>(Uncorrelated) HF results in Ref. 28. Correlated HF results are  $E_G=8.21$  eV in MgO and  $E_G=7.74$  eV in CaO.

<sup>d</sup>Reference 29.

<sup>e</sup>Reference 30.

as

$$\Sigma_{\text{SEX}}(\mathbf{r}, \mathbf{r}') = - \sum_{\mathbf{kn}}^{\text{occ}} \psi_{\mathbf{kn}}(\mathbf{r}) \psi_{\mathbf{kn}}^*(\mathbf{r}') W(\mathbf{r}, \mathbf{r}'; \omega=0), \quad (9)$$

$$\Sigma_{\text{COH}}(\mathbf{r}, \mathbf{r}') = \frac{1}{2} \delta(\mathbf{r}-\mathbf{r}') [W(\mathbf{r}, \mathbf{r}'; \omega=0) - v(\mathbf{r}, \mathbf{r}')], \quad (10)$$

where  $\Sigma_{\text{SEX}}$  is the screened-exchange term and  $\Sigma_{\text{COH}}$  is the Coulomb-hole term which becomes the local potential in the static approximation. The self-energy matrix element of  $W(\mathbf{r}, \mathbf{r}'; \omega=0)$  in the  $d$  orbitals is the Coulomb interaction including the  $d$ - $d$  screening, which will be discussed in the following section.

### B. LMTO minimal basis set and choice of LMTO parameters

Because the plane wave basis becomes very costly for systems containing  $3d$  or  $4f$  electrons, the LMTO method<sup>25</sup> is more appropriate. We use the LMTO basis set  $\chi_{\mathbf{RL}\nu}(\mathbf{r})$  within the atomic sphere approximation (ASA) for the LDA calculation. Here  $L$  is angular momentum  $L = (l, m)$ . The LMTO can be expanded by the muffin-tin orbital  $\phi_{\mathbf{RL}\nu}(\mathbf{r})$  and its energy derivative  $\dot{\phi}_{\mathbf{RL}\nu}(\mathbf{r})$ . The product basis formalism<sup>31</sup> is used and proved to be very efficient. Computational details and numerical technique are shown in Appendixes A and B.

The lattice constants of MgO, CaO, TiO, and VO are  $a = 4.2122, 4.8105, 4.1766,$  and  $4.062$  Å, respectively.<sup>32</sup> Empty spheres (ES's) are often necessarily introduced in the ASA formalism except in closed packing lattices. The calculation of insulating MgO and CaO without ES gives a larger GW band gap by about 1 eV than that of calculation with one ES. In the metallic TiO and VO, proper states are not obtained by the calculation without ES's in the LDA. In the case of two or more ES's in NaCl type structure, the radii of ES become too small. In the calculation with two ES's the band gap is almost the same as in the calculation with one ES. Therefore, the one type of ES is enough in the NaCl type structure. In

the present paper, we use the following sets of radii (in atomic unit) of atomic spheres; (Mg, O, ES)=(2.21, 2.21, 1.62), (Ca, O, ES)=(3.03, 2.19, 1.49), (Ti, O, ES)=(2.71, 1.87, 1.13), and (V, O, ES)=(2.58, 1.91, 1.12). In metallic systems we use 512 ( $8 \times 8 \times 8$ ) mesh points to have enough convergence. On the other hand, in insulating systems smaller number of mesh points 64 ( $4 \times 4 \times 4$ ) is good enough to achieve a convergence because of the existence of the band gap.

We must treat the wide energy range in the calculation of the dielectric function and, therefore, use a sufficient number of LMTO's. The energy-dependent polarization function  $\chi^0(\omega)$  has a long tail in higher energy range and, therefore, metal  $f$  and oxygen  $d$  or  $f$  orbitals are included for the GWA in the present work, though these orbitals are omitted usually in the LDA. The existence of ES is important but higher order orbitals in ES are not essential. The set of the maximum orbitals  $l$  of the LMTO basis in M, O and ES atomic spheres are chosen to be ( $ffs$ ) for MgO, ( $ffd$ ) for CaO, ( $fds$ ) for TiO, and ( $fds$ ) for VO. In CaO, since the band gap becomes narrower, we include the basis of ES with higher angular momentum. There are no essential differences between the different choices but the above choice is the best for the band gap within  $\pm 0.1$  eV.

## III. RESULTS AND DISCUSSIONS

### A. Energy band structure

#### 1. Insulator : MgO and CaO

MgO and CaO are ionic crystals and are band insulators. In MgO, the band gap separates the unoccupied oxygen  $2p$  valence bands and the unoccupied magnesium  $3s$ - $3p$  conduction bands. In CaO the band gap locates between the unoccupied  $4s$ - $4p$  conduction bands and the unoccupied calcium  $3d$  conduction bands. The band structures of MgO and CaO, calculated both in the LDA and the GWA, are shown in Fig. 1 along high symmetry lines. The band gap, the width of the upper

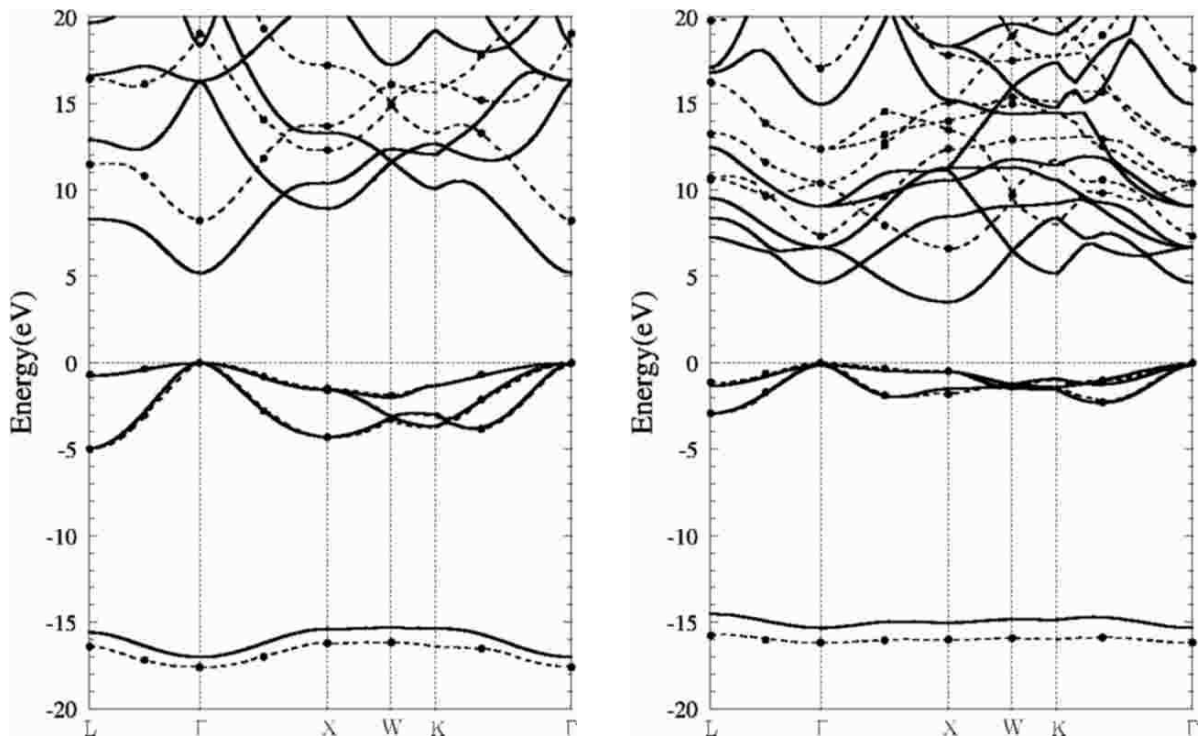


FIG. 1: The energy bands of MgO (left) and CaO (right), calculated by the LDA (solid lines) and the GWA (dashed lines) along high symmetry lines. The closed circles are the calculated points in the GWA. The high symmetry points are  $L=(1/2, 1/2, 1/2)$ ,  $\Gamma=(0, 0, 0)$ ,  $X=(1, 0, 0)$ ,  $W=(1, 1/2, 0)$ , and  $K=(3/4, 3/4, 0)$ .

valence bands and the position of the low lying oxygen  $2s$  band are summarized in Table I, in comparison with those by the LDA and the HF approximation. Our results of MgO are in good agreement with those of the previous GW calculation.<sup>16</sup>

The band gap in the GWA is found to be 8.2 eV in MgO and 6.64 eV in CaO, which are in good agreement with the experimental values 7.8 and 7.1 eV,<sup>29</sup> respectively. The band gap in MgO is the direct one at  $\Gamma$  point both in the LDA and the GWA as in experiments. The band gap in CaO is the indirect one between  $\Gamma$  and  $X$  points in the GWA as in the LDA, although the energy difference between the  $\Gamma$ - $\Gamma$  gap and  $\Gamma$ - $X$  gap becomes smaller in the GWA. The conduction band minimum at the  $X$  point originates from metallic  $d$  states and the lowering the conduction band minimum at the  $X$  point is due to deepening of the potential of the metal ion. On the other hand, the direct gap of CaO at the  $\Gamma$  point was proposed by the HF approximation with correlation calculated by the second order perturbation theory.<sup>28</sup> We are not aware of any angle-resolved photoemission or inverse photoemission experiments on CaO, and the nature of the fundamental gap of CaO cannot be concluded at present.

The GWA valence band width is 5.0 eV in MgO and 2.9 eV in CaO, which are in good agreement with experiments and almost the same as those of the LDA. The LDA valence band width is generally narrower in

general than the GWA and the observation, because the wave functions of valence states are more concentrated on atomic sites by local approximation in the LDA, and the effect of the exchange and correlation effects are much enhanced.<sup>33</sup> However, because the valence bands are oxygen  $2p$  states, such exchange and correlation effects do not affect much in MgO and CaO and band width reduction is not much. In the calculation with the exact-exchange (EXX) potential,<sup>34</sup> the valence band width of MgO and CaO is narrower than the one in the LDA but this is due to the different reason. In the EXX calculation, the exchange energy is approximated by the spherically symmetrized Fock term and the correlation energy is replaced by that of the LDA. The EXX potential is larger in comparison with the LDA exchange potential and gives narrower valence bands of MgO and CaO. In the HF approximation, which includes the non-local interaction, the valence band width is broadened, for instance, in MgO.<sup>26,27</sup> But the band gap and band width are overestimated in the HF approximation due to the lack of screening effects. In the GWA the valence band width is reduced in comparison with the HF method.

The position of oxygen  $2s$  band is pushed down in the GWA so it is close to the experimental value. The LDA makes the core or semicore states locate into shallow energy regions, compared with experiments, because the LDA potential contains self-interaction.

The self-energy and the correction  $Z\Delta\Sigma$  to the LDA

TABLE II: The band width of O  $2p$  band  $W_{2p}$ , the position of O  $s$  band  $E_{O_s}$ , and the band width of transition metal  $3d$  band  $W_{3d}$ ,  $W_{t_{2g}}$ , and  $W_{e_g}$  in metallic TiO and VO. The unit is (eV).

	TiO			VO		
	LDA	COHSEX	GWA	LDA	COHSEX	GWA
$W_{2p}$	4.6	4.7	4.1	5.2	5.3	4.6
$E_{O_s}$	$\sim 22$	$\sim 25$	$\sim 23$	$\sim 22.5$	$\sim 25$	$\sim 23$
$W_{3d}$	8.4	9.1	6.8	8.1	7.6	6.4
$W_{t_{2g}}$	6.5	6.1	4.3	6.4	5.4	3.8
$W_{e_g}$	4.1	4.1	3.2	4.5	4.4	3.3

energy of MgO are shown in the left side of Fig. 2. The gap at the top of the valence bands (the energy zeroth) is seen in the self-energy and as a result the energy correction  $Z\Delta\Sigma$  has the discontinuity. In conduction bands, fluctuations of  $\Sigma^x$  and  $V_{\text{LDA}}^{\text{xc}}$  are caused by different orbital characters, but the correction terms  $Z\Delta\Sigma$  converge to almost constant value. The correction terms of the highest valence band  $Z_{\text{HVB}}$  and those of the lowest conduction band  $Z_{\text{LCB}}$  are as follows: in MgO,  $Z_{\text{HVB}} = 0.75\text{--}0.8$  and  $Z_{\text{LCB}} = 0.83\text{--}0.87$ ; in CaO,  $Z_{\text{HVB}} = 0.73\text{--}0.75$  and  $Z_{\text{LCB}} = 0.80\text{--}0.85$ . The smaller  $Z$  of CaO shows that the electron-electron correlation in CaO is stronger than in MgO.

To see the dynamical screening effects in MgO and CaO, we also calculated the energy band structure by using the static COHSEX approximation and shown in Table I. In the static COHSEX approximation, the band gap is much smaller than the HF results but is still overestimated to be 9.6 eV in MgO and 7.7 eV in CaO. The reduction of the band gap from the HF result to the static COHSEX result and that from the static COHSEX result to the GW result are attributed to the static screening effect and the dynamical screening effect, respectively. Therefore, in MgO and CaO, the static screening is the major contribution rather than the dynamical effects.

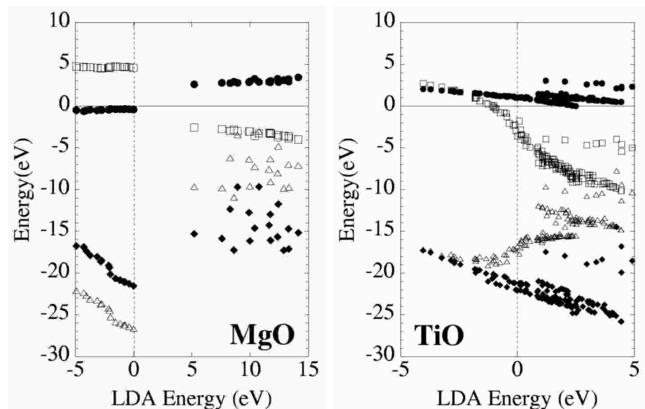


FIG. 2: Energy dependence of the self-energy of MgO (left) and TiO (right). The closed diamond for  $V_{\text{LDA}}^{\text{xc}}$ , the open triangles for  $\Sigma^x$ , the open squares for  $\Sigma^c$ , and the closed circles for  $Z\Delta\Sigma$ .

The valence band width is 5.6 eV in MgO, and 3.4 eV in CaO in the static COHSEX approximation. In the GWA the valence band width is slightly reduced in comparison with the static COHSEX approximation. The reduction from that of the HF approximation to that of the static COHSEX approximation is much larger in MgO, because of the large difference of electronegativity and resultant importance of the static screening. The comparison of the band width by the GWA with that by the static COHSEX approximation clearly shows that the dynamical effects are appreciable in the electron-electron correlation.

## 2. Metal : TiO and VO

TiO and VO are metals, showing typical properties of covalent crystals such as high melting temperature and extreme hardness. The band structures of TiO and VO are shown in Fig. 3, calculated both in the LDA and the GWA and summarized in Table II. In the LDA the oxygen  $2s$  states are located around about 22 eV below  $E_F$  in TiO and VO. These oxygen  $2s$  states are separated by about 11 eV from the bonding states consisting of metal  $3d$  and oxygen  $2p$  orbitals in both TiO and VO, mainly oxygen  $2p$ , at  $7 \sim 10$  eV below  $E_F$ . A real gap of about 2 eV in TiO and that of about 1.5 eV in VO can be seen between this bonding states (mainly oxygen  $2p$ ) and the antibonding states (mainly transition metal  $3d$ ) at around  $E_F$ . The occupied conduction states are heavily dominated by transition metal  $3d$  orbitals.

The band width of metal  $3d$  states becomes narrower in the GWA than in the LDA. The occupied  $3d$  band width from the UPS and XPS is about 3 eV in  $\text{TiO}_{1.03}$ .<sup>35</sup> The width of the unoccupied  $3d$  band in the GWA agrees with that of the BIS spectra.<sup>35</sup>

In TiO and VO the width of oxygen  $2p$  valence band in the GWA becomes narrower in comparison with that of the LDA, which is not the case in MgO and CaO. The hybridization is very small in MgO and CaO. In TiO and VO, the hybridization between the transition metal  $3d$  and oxygen  $2p$  increases due to deepening metal  $3d$  states with the increase of the  $d$  electron. Once one adopts the GWA, the wave functions of valence bands are localized more due to the screening effects and the width of the band around  $-10$  eV becomes narrower. Then the con-

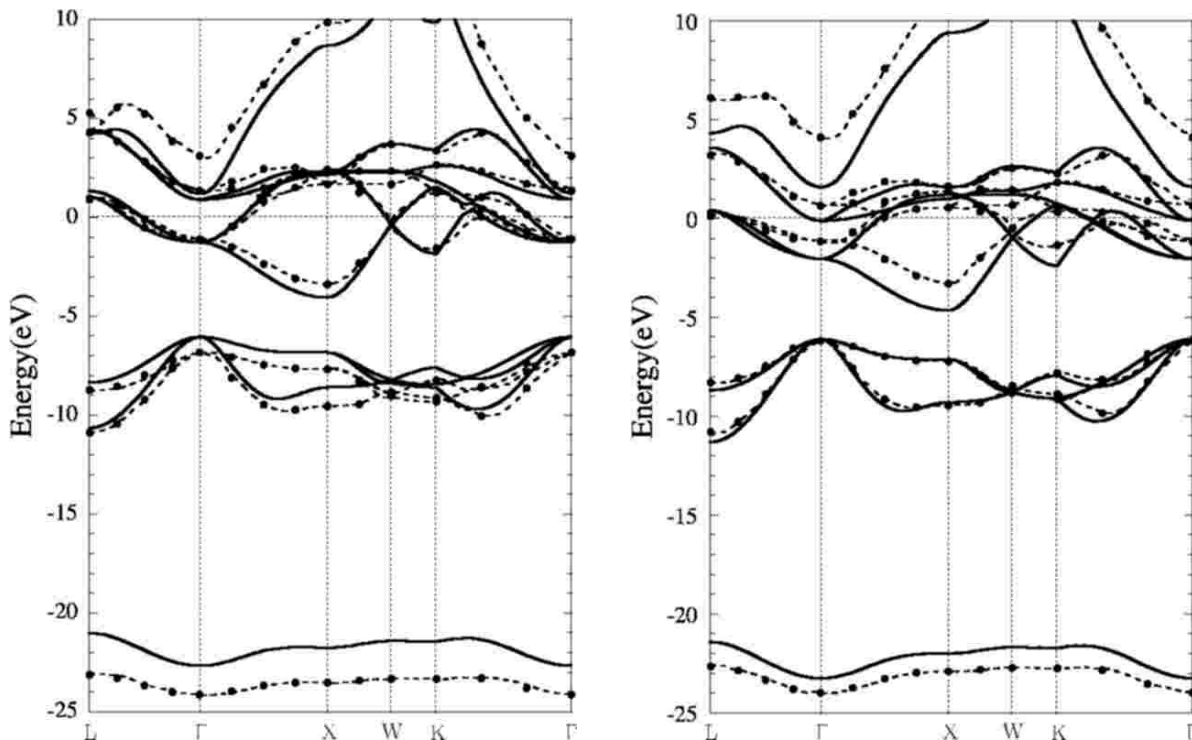


FIG. 3: The energy bands of TiO (left) and VO (right), calculated by the LDA (solid lines) and by the GWA (dashed lines) along high symmetry lines. The closed circles are the calculated points in the GWA. The highest energy band in the figure is mainly from metal  $s$  states. For the symmetry points, see the caption of Fig. 1.

duction bands are lifted to higher energy side, relative to the lower energy oxygen  $2p$  (bonding) band in TiO and VO. The effects of the reduction of the conduction (transition metal  $3d$ ) band width also causes the increasing the separation between  $e_g$  and  $t_{2g}$  states. The position of oxygen  $2s$  band is also pushed down by the GW correction, and this is caused by the self-interaction correction as in MgO and CaO.

The self-energy and the correction  $Z\Delta\Sigma$  to the LDA energy of TiO are shown in the right side of Fig. 2. In contrast to insulating system MgO three parts of the self-energy and the energy correction  $Z\Delta\Sigma$  are continuous at the Fermi energy  $E_F$ , which are the typical properties of the Fermi liquid. The renormalization factor of transition metal  $3d$  states is  $Z = 0.55\text{--}0.65$  in TiO and  $Z = 0.51\text{--}0.63$  in VO.  $Z$  of oxygen  $2p$  states is about  $0.7\text{--}0.8$  in both systems. Those results of the renormalization factor suggest that the interaction between  $3d$  electrons is strong, and the correlation in VO is larger than in TiO.

The  $d$ - $d$  Coulomb interaction  $\langle\phi_d\phi_d|W(\omega=0)|\phi_d\phi_d\rangle$  is calculated to be about  $1.5$  eV both in TiO and VO. The bare Coulomb interaction  $\langle\phi_d\phi_d|v|\phi_d\phi_d\rangle$  is actually  $15.3$  eV in TiO and  $17.8$  eV in VO. Then the correlation term  $\langle\phi_d\phi_d|W^c(\omega=0)|\phi_d\phi_d\rangle$  is  $-13.7$  eV in TiO and  $-16.3$  eV in VO. Therefore, the correlation effects and the static screening (at the Fermi energy) are quite important in these metallic oxides. We should mention that the  $d$ - $d$  Coulomb interaction  $\langle\phi_d\phi_d|W(\omega=0)|\phi_d\phi_d\rangle$

is different from the Hubbard  $U$  evaluated from the LDA, which includes only screening by on-site  $d$  electrons. The term  $\langle\phi_d\phi_d|W(\omega=0)|\phi_d\phi_d\rangle$  includes the screening ef-

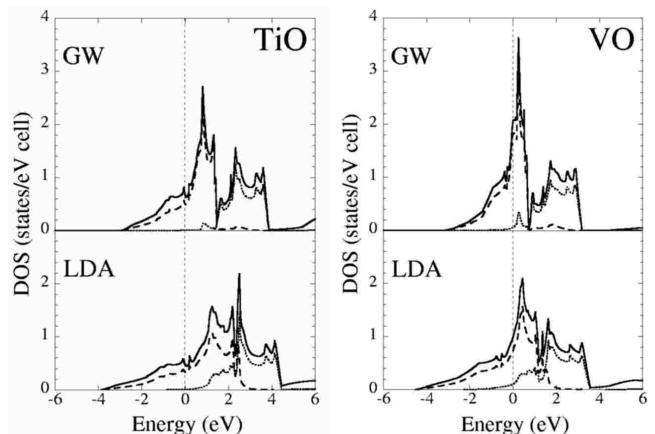


FIG. 4: Total and projected DOS in a transition metal atom in TiO and VO by the LDA (bottom) and the GWA (top). The solid lines for the total DOS in a unit cell, the dotted lines for the partial DOS of transition metal  $3d$ - $e_g$  states and the chain lines for the partial DOS of transition metal  $3d$ - $t_{2g}$  states. The contribution by the oxygen atom is small in this energy range.

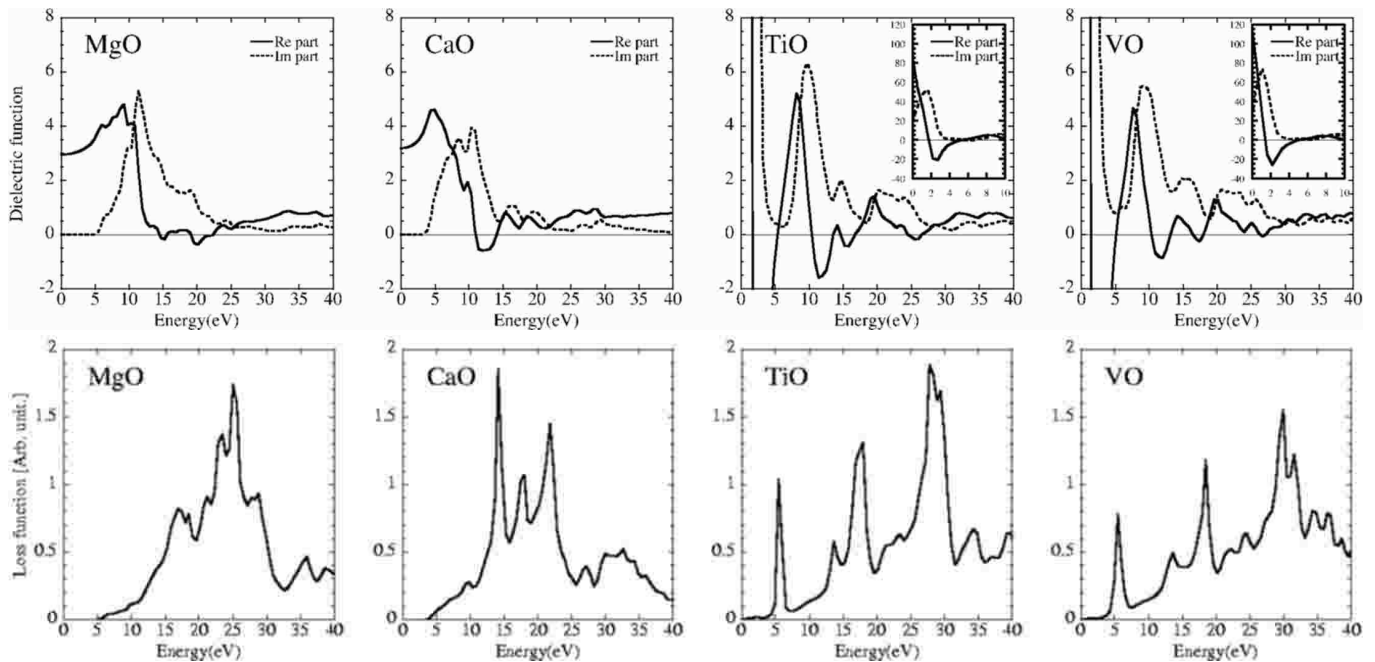


FIG. 5: From left to right, spectra of MgO, CaO, TiO, and VO are shown. Upper panel and lower panel are the dielectric function  $\varepsilon(\omega)$  and the electron energy-loss spectra (EELS)  $\varepsilon^{-1}(\omega)$  for  $\mathbf{q} = 2\pi/a(0.25, 0, 0)$ .

fects by both on-site and off-site  $d$  electrons.<sup>36</sup>

The density of states (DOS) of transition metal  $3d$  orbitals are shown in Fig. 4. In the calculation of the density of states in the present GWA, the eigenvalues were replaced by those of the GWA but the eigenfunctions were the same as those of the LDA, and the lifetime (from imaginary part of the self-energy) of quasiparticle was not considered. The transition metal  $e_g$  states are pushed up in the GWA and the  $e_g$ - $t_{2g}$  separation becomes much clearer than in LDA results.

To see the dynamical correlation effects in TiO and VO we also show the results by the static COHSEX approximation in Table II. The band width of the static COHSEX approximation does not become narrower appreciably in comparison with the LDA results. The reduction by the GWA is much appreciable. We could conclude that the band width reduction is mainly due to the dynamical correlations. The importance of the dynamical correlation was also mentioned in the  $3d$  band width of  $3d$  ferromagnetic transition metals.<sup>11</sup>

Application of the LDA+U method to TiO and VO lead to antiferromagnetic insulators rather than paramagnetic metals, when one uses the  $U$  value obtained by the LDA and the photoemission spectra.<sup>6</sup> However, as already shown, the  $d$ - $d$  Coulomb interaction  $\langle \phi_d \phi_d | W^c(\omega = 0) | \phi_d \phi_d \rangle$  is much smaller by the correlation effects.

## B. Energy loss spectrum and plasmon frequency

The dielectric function is seen in the procedure of the GW calculation. We show the dielectric functions and the electron energy-loss spectra (EELS) in Fig. 5 for  $\mathbf{q} = 2\pi/a(0.25, 0, 0)$ , using 512  $\mathbf{k}$  points in the Brillouin zone.

The dielectric function consists of a part of free electron contribution and a part of interband transition.<sup>37</sup> The plasmon frequency  $\omega_{p1}$  corresponds to the zeroth of the free electron part of the dielectric function and the peak of the EELS. When the interband transition exists at lower energy side of the plasmon frequency, the frequency of vanishing  $\varepsilon(\mathbf{q}, \omega)$  shifts towards higher frequency side. This is the shift of the plasma edge in the dielectric functions of metals or the shift of the plasmon peak in the EELS. The peaks of the imaginary part of the dielectric function  $\varepsilon(\omega)$  appear essentially at the energies of interband excitations. On the other hand, the peaks of the EELS appear at positions where the dielectric function vanishes or becomes very small. Therefore, the EELS have complex structure originated from the situation of the coexistence, in a narrow energy region, of the plasma edge and the interband transition. This is the case in transition metal monoxides and it may be very interesting to see the difference or the similarity of the dielectric functions and the EELS of MgO, CaO, TiO, and VO.

The interband transition from O  $2p$  to metal  $3d$  appears at about 10 eV in CaO, TiO, and VO but that of MgO locates at much higher energy. In MgO, the transition from O  $2p$  to metal  $3s$ - $3p$  creates a broad peak of

$\varepsilon(\omega)$  at about 12 eV. On the other hand, the transition from O  $2p$  to metal  $4s-4p$  makes a structure of  $\varepsilon(\omega)$  at about  $15 \approx 20$  eV in CaO, at about  $20 \approx 27$  eV in TiO and VO. The sharp peaks of  $\varepsilon(\omega)$  at 1.5 eV in TiO and at 1.1 eV in VO are created by metal  $3d-3d$  transition. The dielectric function of metals should reduce generally to zero near  $\omega = 0$  and then show the Drude peak at  $\omega = 0$ . In metallic compounds TiO and VO, low energy excitation peaks of  $\varepsilon(\omega)$  exist down to  $0.2 \approx 0.3$  eV. Then the nonzero value of  $\text{Im}\varepsilon(\omega = 0)$  in Fig. 5 is the artifact caused by broadening these low frequency peaks of the irreducible polarization function  $\chi^0$  by Gaussian with a width of  $\sigma \approx 0.7$  eV.

In the EELS, the sharp peak of metallic TiO and VO at 5 eV is originated from metal  $3d-3d$  transition. The transition from O  $2p$  to metal  $3d$  generates the peak at 14 eV in CaO and at 18 eV in TiO and VO. The shoulder at around 17 eV in MgO is caused by the transition from O  $2p$  to metal  $3s-3p$  because the imaginary part of dielectric function has a relatively large nonzero value at this energy due to broad peak of interband transition. The plasmon peak shifts from 21.1 to 25.0 eV in MgO, from 17.2 to 21.8 eV in CaO, from 24.6 to 27.8 eV in TiO, and from 27.2 to 29.9 eV in VO due to interband transitions. In this estimation of the plasmon frequency, we adopted the number of electrons to be 6 for MgO and CaO (metal  $s$  and O  $2p$  electrons), 8 for TiO (Ti  $3d,4s$  and O  $2p$ ), and 9 for VO (V  $3d,4s$  and O  $2p$ ).

#### IV. SUMMARY

We applied the GWA to the nonmagnetic oxides MgO, CaO, TiO, and VO. Band gap and occupied oxygen  $2p$  band width in insulating MgO and CaO are in good agreement with experimental results. In both systems oxygen  $2s$  level is pushed down, because the self-interaction is corrected in the GWA. We compare the results by the GWA with those by the static COHSEX approximation and discussed the effects of the dynamical correlation. In metallic TiO and VO, the band width of transition metal  $e_g$  and  $t_{2g}$  states become narrower due to the correlation effects.

We also present values of the  $d-d$  Coulomb interaction in TiO and VO and showed the crucial role of the dynamical correlation in these systems. The GW method may be one of the most appropriate method which can provide the information of the electron-electron interaction with screening effects.

The actual wave functions should differ from those in the LDA when the effects of dynamical correlation are included. The choice of the starting wave functions or equivalently the choice of the unperturbed Hamiltonian in the GWA may be very important from this point. This may be very essential for the characteristics in the magnetic transition metal oxides but still open for the future study.

#### Acknowledgments

We thank to F. Aryasetiawan and T. Kotani for useful discussions and suggestion about our GW code development. This work is supported by Grant-in-Aid for COE Research ‘‘Spin-Charge-Photon’’, and Grant-in-Aid from the Japan Ministry of Education, Science, Sports and Culture. Part of the present calculation has been done by use of the facilities of the Supercomputer Center, Institute for Solid State Physics, University of Tokyo.

#### APPENDIX A: COMPUTATIONAL DETAILS

Since the wave function  $\psi$  is written in terms of the LMTO basis functions  $\chi$ , the Hilbert space of the self-energy is spanned by the product basis as

$$\{\Sigma\} = \{\psi\psi\} = \{\chi\chi\} = \{\phi\phi\} + \{\dot{\phi}\dot{\phi}\} + \{\dot{\phi}\dot{\phi}\}. \quad (\text{A1})$$

In the present calculations, because of a proper choice of the energy parameters the absolute values of the mixing coefficients of  $\dot{\phi}$  to  $\phi$  are less than 0.1 for all terms and the norm of  $\dot{\phi}$ ,  $\langle\dot{\phi}\dot{\phi}\rangle$ , is  $0.1 \sim 0.3$  even in the largest case. Then the terms including  $\dot{\phi}$  can be dropped out safely and the self-energy  $\Sigma$  can be expanded by  $\phi_{l'm'\nu'}^*(\mathbf{r})\phi_{lm\nu}(\mathbf{r}) = \phi_{l'\nu'}(|\mathbf{r}|)\phi_{l\nu}(|\mathbf{r}|)Y_{l'm'}^*(\hat{\mathbf{r}})Y_{lm}(\hat{\mathbf{r}})$ . The product of two spherical harmonics is reduced to the linear combination of one spherical harmonics. Consequently we can construct the new basis set

$$\begin{aligned} & \tilde{B}_{\mathbf{R}l'\nu';l''m''}^{\mathbf{k}}(\mathbf{r}_{\mathbf{R}}) \\ &= \sum_{\mathbf{T}} e^{i\mathbf{k}\cdot\mathbf{T}} \phi_{l'\nu'}(|\mathbf{r}_{\mathbf{R}\mathbf{T}}|)\phi_{l\nu}(|\mathbf{r}_{\mathbf{R}\mathbf{T}}|)Y_{l'm''}(\widehat{\mathbf{r}_{\mathbf{R}\mathbf{T}}}), \end{aligned} \quad (\text{A2})$$

where  $L''$  is depend on  $l'$  and  $l$ , that is  $|l-l'| \leq l''(l', l) \leq l+l'$  and  $|m''(l', l)| \leq l''(l', l)$ , and  $\mathbf{r}_{\mathbf{R}\mathbf{T}} = \mathbf{r} - \mathbf{R} - \mathbf{T}$ . The orthonormal basis set  $B$  can be produced by the linear combination of the nonorthogonal basis set  $\tilde{B}$  as  $B_i^{\mathbf{k}} = \sum_j \tilde{B}_j^{\mathbf{k}} D_{ji}^{\mathbf{k}}$ , where  $j = (\mathbf{R}l'\nu';l''m'')$ ,  $i$  is a new suffix in the orthonormal basis set and  $D$  is the transformation matrix from the nonorthogonal basis to the orthonormal basis. Here we use the convenient notation

$$|B_i^{\mathbf{k}}\rangle \equiv |i_{\mathbf{k}}\rangle = |\tilde{i}_{\mathbf{k}}\rangle D^{\mathbf{k}}, \quad |\tilde{i}_{\mathbf{k}}\rangle \equiv |\tilde{B}_i^{\mathbf{k}}\rangle. \quad (\text{A3})$$

The matrix  $D^{\mathbf{k}}$  is obtained by orthogonalizing the overlap matrix  $O_{ij}^{\mathbf{k}} = \langle\tilde{i}_{\mathbf{k}}|\tilde{j}_{\mathbf{k}}\rangle$ .

We can expand the self-energy in terms of the new orthonormal basis set  $|i_{\mathbf{k}}\rangle$ . To calculate the self-energy we first calculate the polarization function  $\chi^0$  with the nonorthonormal basis.

The Coulomb potential is calculated by using the bare structure constant of the LMTO method.<sup>38</sup> In this method, two parts of the Coulomb matrix can be calculated separately, on-site and off-site parts, by using the LMTO bare structure constant  $S^0(\mathbf{q})$ .

Next we need to transform from nonorthonormal basis  $|\tilde{i}_{\mathbf{k}}\rangle$  to orthonormal basis  $|i_{\mathbf{k}}\rangle$ , that is  $\langle\tilde{i}|\chi^0|\tilde{j}\rangle \rightarrow \langle i|\chi^0|j\rangle$

and  $\langle \tilde{i}|v|\tilde{j} \rangle \rightarrow \langle i|v|j \rangle$ . Within the orthonormal basis we can calculate the response function  $\chi = (1 - \chi^0 v)^{-1} \chi^0$  and the screened Coulomb potential  $W^c = v\chi v$ . Finally the self-energy can be obtained by the inverse transformation from the orthogonal basis to the nonorthogonal basis, and that from the product basis to the Bloch basis.

The number of basis set can be reduced by excluding terms of higher  $l''$ . We have studied the dependence on a choice of the maximum  $l''$ 's for set of  $l''$  in (Mg, O, ES) atomic spheres being (3,3,0), (4,4,0) and (6,6,0). The configuration (6,6,0) corresponds to the full calculation for orbital  $f$  for metals,  $f$  for oxygen and  $s$  for ES. The total number of product bases of (3,3,0), (4,4,0), and (6,6,0) are 120, 174, and 222, respectively. The proper choice may be a set of the maximum  $l''$ 's which produces the total number of the product basis nearly equals to a half of that in the maximum choice. For example, the product basis of (3,3,0) may be enough for the set of the  $ffs$  Bloch orbitals. In present work the full product basis is selected, but this way of product basis reduction is very effective and powerful for large systems.

## APPENDIX B: NUMERICAL TECHNIQUE

In the calculation of the self-energy, the integration is performed over the whole Brillouin zone. The Coulomb

matrix  $v(\mathbf{q})$  has a singularity at  $\mathbf{q} = 0$  as  $F(\mathbf{q}) = 1/|\mathbf{q}|^2$ . The integration of  $v(\mathbf{q})$  over the Brillouin zone does not diverge but special cares are needed not only for the  $\mathbf{q} = 0$  term but for small finite  $\mathbf{q}$ . In the present calculation, the integration over the Brillouin zone is replaced by the summation over discrete points. We use a set of discrete points distributed densely near the  $\mathbf{q} = 0$  point, not on uniform  $\mathbf{k}$  mesh, in the Brillouin zone. For a choice of the discrete points near  $\mathbf{q} = 0$ , we use the offset  $\Gamma$ -point method.<sup>39</sup> The integration of  $F(\mathbf{q})$  over the Brillouin zone can be performed analytically and the offsetted points  $\mathbf{Q}$ 's are chosen near  $\mathbf{q} = 0$  so as to satisfy a relation

$$\int_{\text{BZ}} F(\mathbf{q}) d\mathbf{q} = \sum_{\mathbf{Q}} F(\mathbf{Q}) + \sum_{\mathbf{k} \neq 0} F(\mathbf{k}), \quad (\text{B1})$$

where  $\mathbf{k}$ 's are the discrete mesh points of the Brillouin zone. The choice of the offsetted points  $\mathbf{Q}$  are taken into consideration so as to keep the symmetry of the system.

We tested the offset method in the exchange energy of the electron gas system and the accuracy has been confirmed even in case of small number of  $\mathbf{k}$ -mesh points. The careful treatment of the Coulomb matrix at or near  $\mathbf{q} = 0$  is very crucial near the band gap or the Fermi level.

---

\* Electronic address: yama@coral.t.u-tokyo.ac.jp  
 † Electronic address: fujiwara@coral.t.u-tokyo.ac.jp;  
 URL: <http://fujimac.t.u-tokyo.ac.jp/FujiwaraLab/index.html>  
<sup>1</sup> P. Hohenberg and W. Kohn, Phys. Rev. **136**, B864 (1964); W. Kohn and L. J. Sham, *ibid.* **140**, A1133 (1965); R. O. Jones and O. Gunnarsson, Rev. Mod. Phys. **61**, 689 (1989).  
<sup>2</sup> K. Terakura, A. R. Williams, T. Oguchi, and J. Kübler, Phys. Rev. Lett. **52**, 1830 (1984); K. Terakura, T. Oguchi, A. R. Williams, and J. Kübler, Phys. Rev. B **30**, 4734 (1984).  
<sup>3</sup> Y. Ishii, in *Computational Physics as a New Frontier in Condensed Matter Research*, edited by H. Takayama, M. Tsukada, H. Shiba, F. Yonezawa, M. Imada, and Y. Okabe (The Physical Society of Japan, Tokyo, 1995), pp. 57–66.  
<sup>4</sup> M. Arai and T. Fujiwara, Phys. Rev. B **51**, 1477 (1995).  
<sup>5</sup> A. Svane and O. Gunnarsson, Phys. Rev. Lett. **65**, 1148 (1990).  
<sup>6</sup> V. I. Anisimov, J. Zaanen, and O. K. Andersen, Phys. Rev. B **44**, 943 (1991).  
<sup>7</sup> V. I. Anisimov, I. V. Solovyev, M. A. Korotin, M. T. Czyzyk, and G. A. Sawatzky, Phys. Rev. B **48**, 16 929 (1993); A. I. Liechtenstein, V. I. Anisimov, and J. Zaanen, *ibid.* **52**, R5467 (1995).  
<sup>8</sup> V. I. Anisimov, F. Aryasetiawan, and A. I. Liechtenstein, J. Phys.: Condens. Matter **9**, 767 (1997).  
<sup>9</sup> L. Hedin and S. Lundqvist, in *Solid State Physics*, edited by H. Ehrenreich, F. Seitz, and D. Turnbull (Academic Press, New York, 1969), Vol. 23, P.1.  
<sup>10</sup> F. Aryasetiawan and O. Gunnarsson, Rep. Prog. Phys. **61**,

237 (1998).  
<sup>11</sup> M. M. Steiner, R. C. Albers, and L. J. Sham, Phys. Rev. B **45**, 13272 (1992).  
<sup>12</sup> D. R. Penn, Phys. Rev. Lett. **42**, 921 (1979); A. Liebsch, Phys. Rev. B **23**, 5203 (1981).  
<sup>13</sup> J. E. Northrup, M. S. Hybertsen, and S. G. Louie, Phys. Rev. Lett. **59**, 819 (1987); J. E. Northrup, M. S. Hybertsen, and S. G. Louie, Phys. Rev. B **39**, 8198 (1989).  
<sup>14</sup> M. S. Hybertsen and S. G. Louie, Phys. Rev. B **34**, 5390 (1986).  
<sup>15</sup> R. W. Godby, M. Schlüter, and L. J. Sham, Phys. Rev. B **37**, 10 159 (1988).  
<sup>16</sup> U. Schönberger and F. Aryasetiawan, Phys. Rev. B **52**, 8788 (1995).  
<sup>17</sup> F. Aryasetiawan, Phys. Rev. B **46**, 13 051 (1992).  
<sup>18</sup> F. Aryasetiawan and O. Gunnarsson, Phys. Rev. Lett. **74**, 3221 (1995).  
<sup>19</sup> S. Massidda, A. Continenza, M. Posternak, and A. Baldereschi, Phys. Rev. Lett. **74**, 2323 (1995).  
<sup>20</sup> S. Massidda, A. Continenza, M. Posternak, and A. Baldereschi, Phys. Rev. B **55**, 13 494 (1997).  
<sup>21</sup> A. Continenza, S. Massidda, and M. Posternak, Phys. Rev. B **60**, 15 699 (1999).  
<sup>22</sup> A. Fujimori and F. Minami, Phys. Rev. B **30**, 957 (1984).  
<sup>23</sup> G. Baym and L. P. Kadanoff, Phys. Rev. **124**, 287 (1961); G. Baym, *ibid.* **127**, 1391 (1962).  
<sup>24</sup> W.-D. Schöne and A. G. Eguluz, Phys. Rev. Lett **81**, 1662 (1998). In this paper fully self-consistent GW calculation is applied to K and Si, and it gives wider band width in K or overestimated band gap in Si.

- <sup>25</sup> O. K. Andersen, Phys. Rev. B **12**, 3060 (1975).
- <sup>26</sup> S. T. Pantelides, D. J. Mickish, and A. B. Kunz, Phys. Rev. B **10**, 5203 (1974).
- <sup>27</sup> T. Bredow and A. R. Gerson, Phys. Rev. B **61**, 5194 (2000).
- <sup>28</sup> R. Pandey, J. E. Jaffe, and A. B. Kunz, Phys. Rev. B **43**, 9228 (1991).
- <sup>29</sup> R. C. Whited, C. J. Flaten, and W. C. Walker, Solid State Commun. **13**, 1903 (1973).
- <sup>30</sup> S. P. Kowalczyk, F. R. McFeely, L. Ley, V. T. Gritsyna, and D. A. Shirley, Solid State Commun. **23**, 161 (1977).
- <sup>31</sup> F. Aryasetiawan and O. Gunnarsson, Phys. Rev. B **49**, 16 214 (1994).
- <sup>32</sup> R. W. G. Wyckoff, *Crystal Structures* (Wiley, New York, 1963).
- <sup>33</sup> E. L. Shirley, Phys. Rev. B **58**, 9579 (1998).
- <sup>34</sup> T. Kotani, Phys. Rev. B **50**, 14 816 (1994); **51**, 13 903(E) (1995); T. Kotani and H. Akai, *ibid.* **54**, 16 502 (1996).
- <sup>35</sup> S. R. Barman and D. D. Sarma, Phys. Rev. B **49**, 16 141 (1994).
- <sup>36</sup> M. Springer and F. Aryasetiawan, Phys. Rev. B **57**, 4364 (1998).
- <sup>37</sup> H. Ehrenreich and H. R. Philipp, Phys. Rev. **128**, 1622 (1962).
- <sup>38</sup> A. Svane and O. K. Andersen, Phys. Rev. B **34**, 5512 (1986).
- <sup>39</sup> T. Kotani and M. van Schilfgaarde (private communications).